Tetrahedron 73 (2017) 1098–1104

Contents lists available at ScienceDirect

Tetrahedron

journal homepage: www.elsevier.com/locate/tet

An investigation of the role the donor moiety plays in modulating the efficiency of 'donor-π-acceptor-π-acceptor' organic DSSCs

Kwang-Won Park [a, 1], Luis A. Serrano [b, 1], Sungwoo Ahn [a], Myung Hoon Baek [a], Alan A. Wiles [b], Graeme Cooke [b, *], Jongin Hong [a, **]

[a] Department of Chemistry, Chung-Ang University, Seoul, 06974, Republic of Korea
[b] WestCHEM, School of Chemistry, University of Glasgow, Glasgow, G12 8QQ, UK

ARTICLE INFO

Article history:
Received 7 August 2016
Received in revised form
21 December 2016
Accepted 23 December 2016
Available online 14 January 2017

Keywords:
Dye-sensitized solar cell
Organic photosensitizer
Donor
Benzothiadiazole

ABSTRACT

Three 'D-π-A-π-A' based dyes have been synthesized featuring MeO-, MeS- and Me_2N- as donor residues and benzothiadiazole and cyanoacrylic acid residues as acceptor units. UV–vis spectroscopy, solution electrochemistry and DFT modelling indicated that the Me_2N- residue has the most significant effect on optical and redox properties of a photosensitizer. DSSCs with the Me_2N- functionalized dye gave the highest power conversion efficiency of the series ($\eta = 5.61\%$), presumably due to the better donor ability of this unit, which promotes more effective intramolecular charge transfer (ICT) characteristics.

1. Introduction

Dye-sensitized solar cells (DSSCs)[1] continue to be intensively studied as potential alternatives to silicon-based photovoltaic devices due to their distinctive features including low cost fabrication and ability to function under low-light conditions.[2] In particular, metal-free organic photosensitizers for DSSCs have become increasingly attractive and offer several advantages over their transition metal-incorporating brethren including cost-effective modular synthesis and higher molar extinction coefficients.[3] The majority of organic dyes reported to date feature a donor-π bridge-acceptor (D-π-A) architecture,[4] with triarylamine-based moieties being commonly used as the D moiety because of their convenient synthesis and interesting electron donating properties.[5] Cyanoacrylic acid residues have been used extensively as the A unit due to their facile synthesis from aldehyde residues and ability to simultaneously act as a TiO_2 anchoring unit. Various π-conjugated bridging units including aromatic, heteroaromatic or alkyne residues have been introduced to induce efficient charge separation between D and A units.[6] Recently, additional subordinate A units,[7] such as benzothiadiazole, have been incorporated as an electron trap to promote charge separation and electron migration to the second A unit in a D-π-A-π-A structure.[8]

In the D-π-A structure, the D units play an important role in determining the optical characteristics of the dye and, as a result, research has been diverted towards investigating the role differing D units have in modulating the absorption characteristics of the dyes and DSSC performance.[9] In this study, we report the facile synthesis of three 'D-π-A_1-π-A_2' organic dyes (**LS-385**, **LS-386** and **LS-387**, Scheme 1). In order to promote planarity between the D and A_1 residues an acetylene linker group has been included.[10] We have also investigated how the differing D groups (MeO-, MeS- and Me_2N-) affect the properties of their parent dyes and resulting DSSC devices.

2. Results and discussion

2.1. Synthesis

The three dyes were synthesized according to Scheme 1. Sonogashira reactions provided the building blocks **3**, **6** and **9** in respectable yields. Suzuki coupling reactions with 4-formylphenyl boronic acid provided the aldehyde-functionalized units (**4**, **7** and

* Corresponding author.
** Corresponding author.
E-mail addresses: Graeme.Cooke@glasgow.ac.uk (G. Cooke), hongj@cau.ac.kr (J. Hong).
[1] These authors made equal contribution to this article.

http://dx.doi.org/10.1016/j.tet.2016.12.061

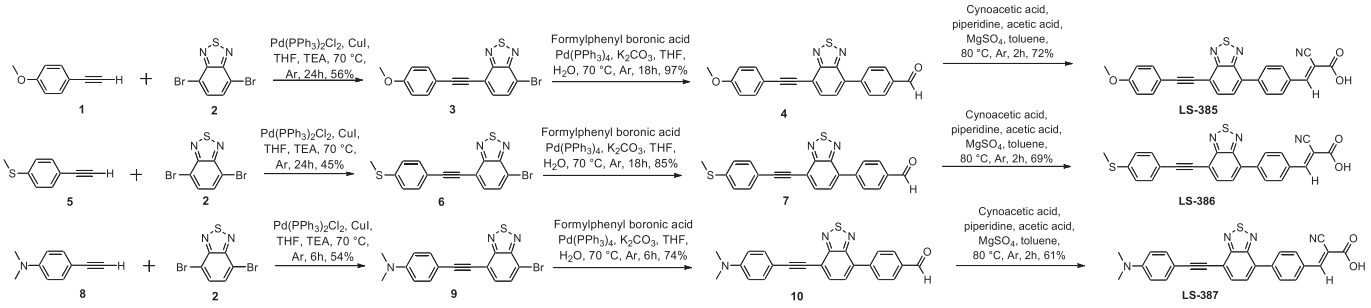

Scheme 1. Synthesis of dyes.

10) in good yields, which upon subsequent Knoevenagel condensation with cyanoacetic acid, yielded dyes **LS-385**, **LS-386** and **LS-387** in respectable yields.

2.2. Characterization

Fig. 1 shows the UV–vis absorption spectra of the three dyes in DMF solution and deposited as TiO_2 films. The absorption band around 300 nm is likely due to a π-π* transition of the conjugated aromatic moieties, and the molar extinction coefficient for this wavelength decreases in the order of **LS-387** > **LS-386** > **LS-385**. The distinct absorption band in the visible region is attributed to the intramolecular charge transfer (ICT) between the D and A moieties. The stronger electron donating ability of the Me_2N- moiety induces a bathochromic shift in the longest wavelength absorption of around 45 nm. This is also confirmed by electronic absorption spectra from the TDDFT calculations (see Supporting Information, Fig. S1). Compared with the spectra in DMF solution, the absorption bands of the dyes adsorbed onto TiO_2 exhibit significant spectral broadening and larger red-shifts because of the interaction of the anchoring groups with the surface of TiO_2 and the *J*-aggregation of photosensitizer molecules. This trend follows the order **LS-387** > **LS-386** > **LS-385**.

The electrochemical behavior of the three compounds was explored by cyclic voltammetry (CV) and square wave voltammetry (SWV) (Supporting Information, Fig. S2). The SWV experiments provided the estimated ionization potential (IP) and electron affinity (EA) energies in Table 1.[11] The E_{fund} (E_{fund} = IP − EA) of **LS-385** and **LS-386** are similar (2.5 eV), however, dye **LS-387** possesses a lower value of 2.22 eV, presumably due to the stronger electron donating nature of the Me_2N- residue.

Table 1
SWV derived redox potentials of the dyes and their estimated EA/IP energies.

Dyes	E_{red}(V)	E_{ox}(V)	EA (eV)	IP (eV)
LS-385	−1.66	0.79	−3.14	−5.59
LS-386	−1.57	0.80	−3.23	−5.60
LS-387	−1.68	0.41	−3.12	−5.21

2.3. Theoretical calculations

DFT and TDDFT calculations were performed to understand the electronic structure and optical properties of the dyes. We defined six bond lengths denoted as d_1 to d_6 to point out the relationship between bond length and electron donating ability for the given molecule (Fig. 2). Table 2 summarizes these bond lengths from the ground state optimized geometries. Among them, d_1 values between molecules differ significantly because of the various atomic radii of oxygen, sulfur and nitrogen. These d_1 values are very consistent with the covalent bonding radius of C–O (1.421 Å),[12] C–N (1.471 Å)[13] and C–S (1.77 Å)[14] single bonds in ascending order. Relatively short bond lengths in the DFT calculations might originate from hybridization between sp^2 and sp^3 carbons.[15] Recently, we reported that bond length values obtained from DFT calculations have strong correlation with the electronic and optical properties as well.[16] Interestingly, **LS-387** has the shortest bond lengths of d_2 to d_6, compared with those of other dyes, whereas no apparent difference between **LS-385** and **LS-386** was observed. We think that such a change in bond length is related to the donor strength of nitrogen, implying extensive delocalization throughout the molecule.[16,17] Accordingly, **LS-387** is expected to result in the best DSSC performance of this series of dyes.

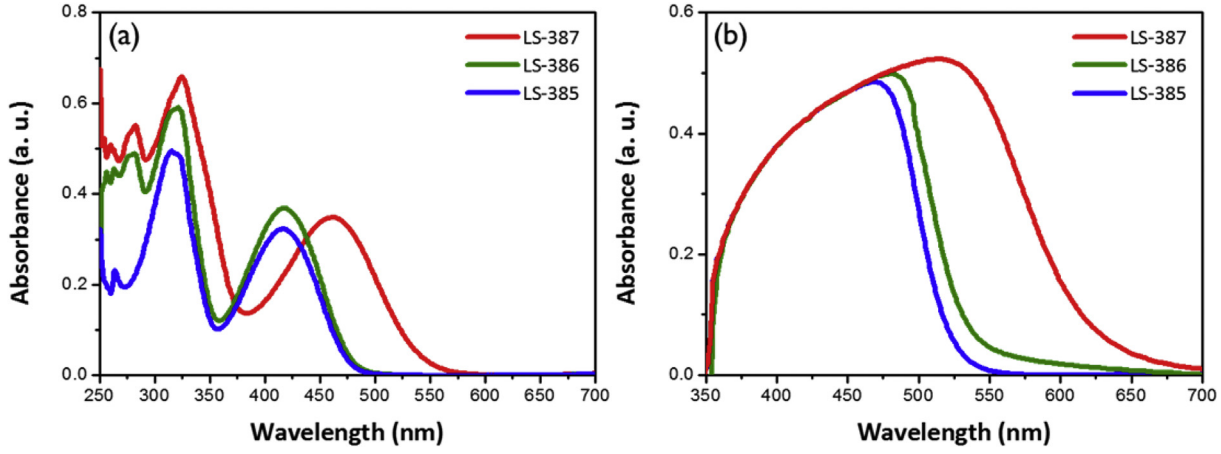

Fig. 1. UV–vis absorption spectra of each dye (a) in DMF solution (1×10^{-5} mol L^{-1}) and (b) adsorbed onto transparent TiO_2 film.

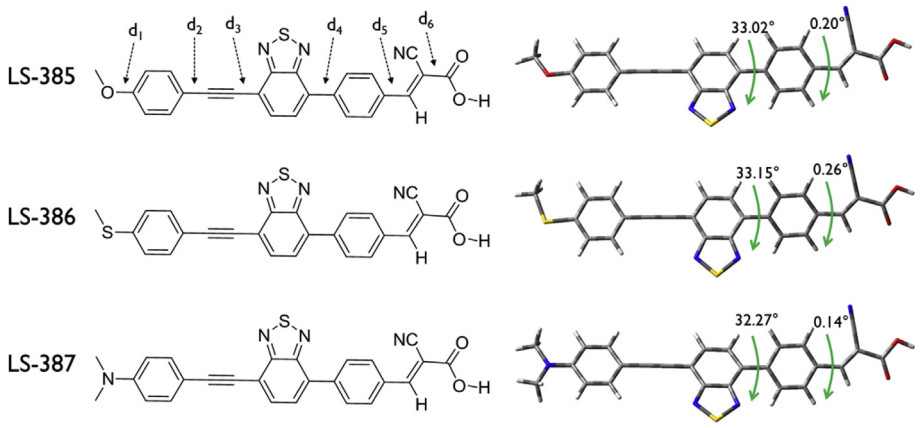

Fig. 2. Molecular structures and ground-state optimized geometry of each dye: (a) **LS-385**, (b) **LS-386**, and (c) **LS-387**. DFT calculations were performed at the 6-311G (d, p) level.

Table 2

Dyes	d_1 (Å)	d_2 (Å)	d_3 (Å)	d_4 (Å)	d_5 (Å)	d_6 (Å)
LS-385	1.35757	1.41749	1.41028	1.47561	1.44805	1.49356
LS-386	1.77654	1.41739	1.41056	1.47576	1.44832	1.49385
LS-387	1.37597	1.41385	1.40799	1.47481	1.44715	1.49278

In the optimized structure, the acetylene bridge is crucial to maintain the coplanar geometry between donor and benzothiadiazole (BTD) units. The cyanoacrylic acid group is found to be fully coplanar with the adjacent phenyl group (π-bridge). Importantly, because of the electron-deficient character of BTD, we employed the phenyl π-linker between BTD and cyanoacrylic acid in order to avoid the electron recombination between TiO_2 and dye cation.[7] However, the dihedral angle between BTD and adjacent phenyl is about 33°, presumably due to steric hindrance between the unpaired electrons of the nitrogen in the BTD unit and hydrogen atoms of the phenyl group.

For an effective photosensitizer in DSSCs, the LUMO of the dye should be located above the TiO_2 conduction band (CB) and its HOMO should be below the iodide redox potential. Fig. 3 shows the isodensity plots of the frontier molecular orbitals of the three dyes (**LS-385**, **LS-386** and **LS-387**). The HOMO and HOMO-1 are delocalized over the entire molecule (including the D unit), whereas the LUMO and LUMO+1 are mainly localized on the A group, with a considerable amount extending onto the π-bridges. Therefore, the photo-induced ICT is likely to occur from D to the TiO_2 surface via the cyanoacrylic acid unit. The calculated energy levels of the three organic dyes reveal an interesting trend as the LUMO levels are similar (−3.13 eV, −3.18 eV and −3.01 eV for **LS-385**, **LS-386** and **LS-387**, respectively), whereas their HOMO levels are significantly different (−5.80 eV, −5.78 eV and −5.34 eV for **LS-385**, **LS-386** and **LS-387**, respectively). The trend in HOMO confirms the stronger electron donating ability of the Me_2N- unit over the other moieties (in agreement with UV–vis and electrochemical data). The extent of ICT can be quantitatively estimated from the NBO analysis[16] and the difference of dipole moment between ground and excited states.[18] The natural charges for donor, π-spacer, and acceptor (denoted as q^{Donor}, $q^{\pi\text{-}spacer}$, and $q^{Acceptor}$, respectively) are summarized in Table S1. It is clear that for **LS-387** more positive natural charges are located on the electron donor, whereas the negative charges reside on the electron acceptor(s). The calculated values for dipole moments are listed in Table S2. The dipole moments in the ground state and the excited state are obtained by DFT and TDDFT calculations, respectively. These results reveal that the strong donating group (Me_2N- in **LS-387**) would more effectively promote the charge separation between the donor and acceptor group of the organic dyes.

2.4. Photovoltaic performance

Fig. 4(a) shows *J-V* characteristics of DSSCs fabricated from the three dyes compared to those produced from **N719** as control. The photovoltaic parameters are summarized in Table 3. The stronger donating ability of Me_2N- resulted in better photovoltaic performance (e.g. power-conversion-efficiency (η), V_{oc} and J_{sc}) compared to the other dyes in this series. The photovoltage depends on the Fermi level for electrons after electron injection among the dyes. After dye sensitization on the TiO_2 surface, a shift in the conduction band edge can occur.[19] The shift is sensitive to the dipole moment of the adsorbed dye and a dye with larger dipole moment yields a larger shift in the conduction band edge, leading to the higher value of V_{oc}. Interestingly, the tendency of V_{oc} follows that of the calculated dipole moments in Table S2. Fig. 4(b) shows incident photon-to-current efficiency (IPCE) spectra for DSSCs according to the following equation:

$$\mathrm{IPCE} = \frac{1240\ (\mathrm{eV\cdot nm})\cdot J_{sc}(\mathrm{mA\cdot cm^{-2}})}{\lambda\ (\mathrm{nm})\cdot\varphi(\mathrm{mW\cdot cm^{-2}})}$$

where J_{sc} is the short-circuit photocurrent density for monochromatic irradiation, λ and φ are the wavelength and the intensity of the monochromatic light, respectively. The IPCE of **LS-387** displays a broader band between 300 nm and 800 nm than that of **LS-385** and **LS-386**. The aforementioned results demonstrate that the Me_2N- moiety broadens the visible absorption spectrum both in solution and upon deposition onto TiO_2. We think that this could be responsible for the significant enhancement of DSSC performance (η = 2.68% for **LS-385**, 2.69% for **LS-386**, and 5.61% for **LS-387**).

Fig. 5 shows the Nyquist plots to study the interfacial charge transfer processes of DSSCs under illumination or in the dark. The first semicircle in the high frequency region is assigned to the redox reaction of I^-/I_3^- at the counter electrode/electrolyte interface. The second semicircle in the intermediate frequency region represents the charge recombination between electrons in the TiO_2 photoanode with I_3^- ions in the electrolyte. The radius of the second semicircle, which is related to the charge recombination rate, increases in the order of **LS-387** < **LS-386** < **LS-385** under illumination and in the dark (*i.e.* a larger radius indicates a slower charge recombination). Interestingly, the impedance in mid-frequency regime under illumination is much smaller than that in the dark because of the difference in the local I_3^- concentration.[20] It should

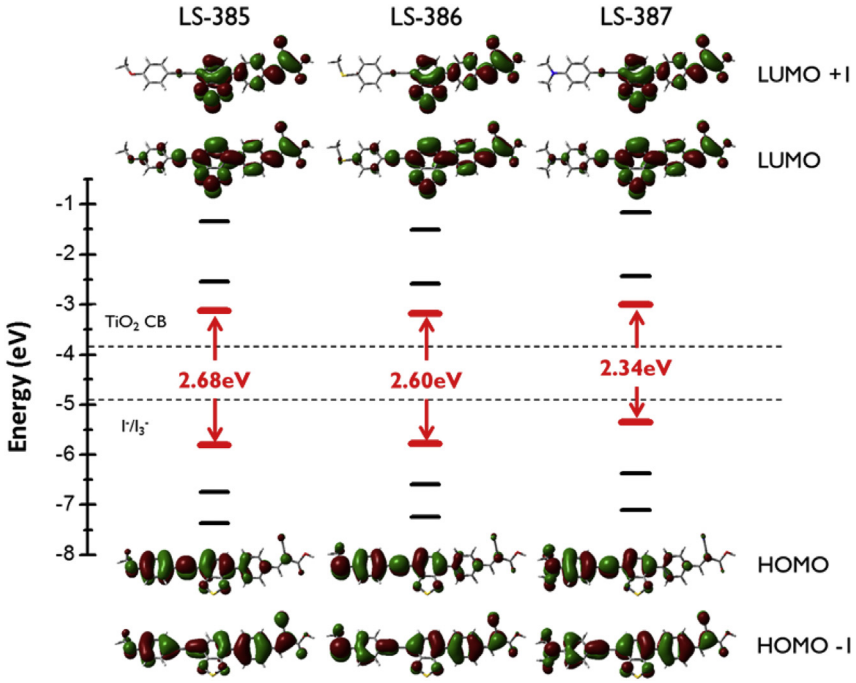

Fig. 3. Frontier molecular orbital energies of each dye and their position relative to the TiO_2 conduction band and I^-/I_3^- redox potential.

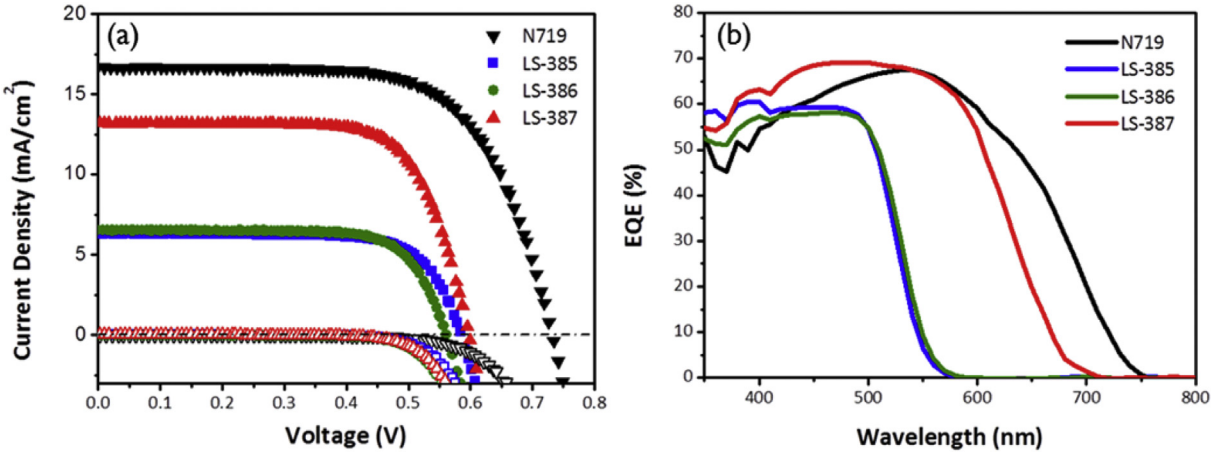

Fig. 4. (a) J-V curves of the organic dye-sensitized DSSCs (**N719**: black, **LS-385**: blue, **LS-386**: green, **LS-387**: red) under one sun illumination (solid) and in dark (hollow) and (b) their IPCE spectra.

Table 3
DSSC performance parameters of all dyes.

Dyes	V_{oc} (V)	J_{sc} (mA/cm^2)	FF	η(%)
N719	0.729	16.76	66.8	8.16
LS-385	0.582	6.33	72.73	2.68
LS-386	0.561	6.53	73.42	2.69
LS-387	0.595	13.26	71.15	5.61

be noted that more I_3^- formation would result from more dye regeneration at the TiO_2/dye/electrolyte interface under illumination. Although **LS-387** is not good at suppressing the back charge recombination at the TiO_2/dye/electrolyte, the highest power conversion efficiency ($\eta = 5.61\%$) can be achieved by its excellent light harvesting and electron injection abilities.

3. Experimental

3.1. General

NMR spectroscopy was recorded on a Bruker AVIII (400 MHz) spectrometer. Chemical shifts are reported in ppm and are relative to TMS. UV–Vis spectra were recorded on a JASCO UV/Vis/NIR spectrophotometer. MS were either recorded on a Thermo Scientific LTQ Orbitrap XL using nanoelectrospray (negative mode, nESI$^-$) or a JEOL-700 MStation (EI). IR spectra were recorded on a Perkin-Elmer FT-IR and transmittance maxima are reported in wavenumbers (cm^{-1}). Cyclic voltammetry measurements were undertaken using a CH Instruments 440 A electrochemical analyzer using a platinum working electrode, a platinum wire counter electrode and a silver wire pseudo-reference electrode. Ferrocene was used as an internal standard and all redox couples are reported

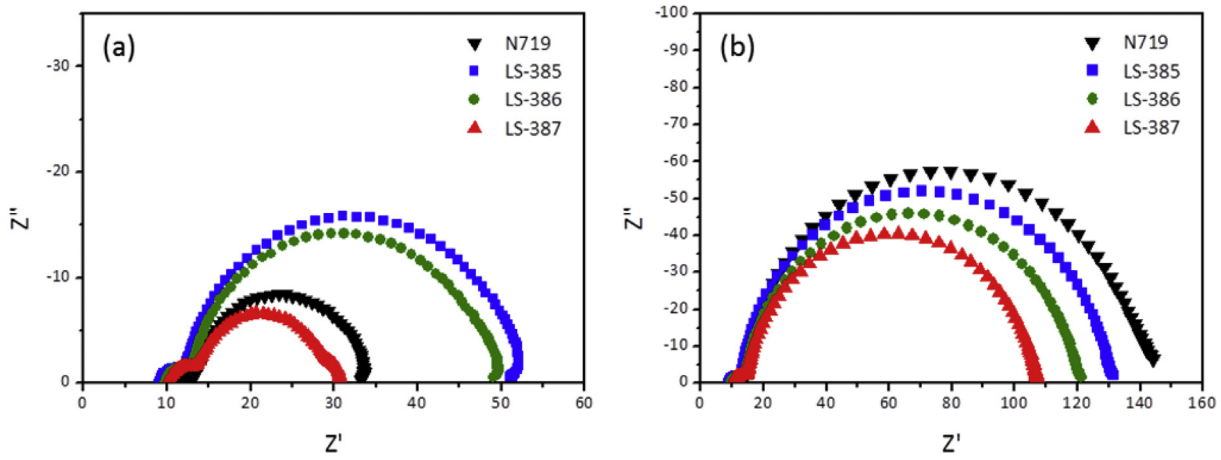

Fig. 5. Nyquist plots of the organic dye-sensitized DSSCs (**N719**: black, **LS-385**: blue, **LS-386**: green, **LS-387**: red) (a) under one sun illumination and (b) in dark.

versus the ferrocene/ferrocenium (Fc/Fc^+ = 4.8 eV) redox couple (adjusted to 0.0 V). The solutions were prepared using dry dimethylformamide (DMF) containing electrochemical grade tetrabutylammonium hexafluorophosphate (0.1 M) as the supporting electrolyte. The solutions were purged with nitrogen gas for 3 min prior to recording the electrochemical data.

3.2. Synthesis

3.2.1. Compound **3**

Compound **2**[21](1.67 g, 5.67 mmol) and 1-ethynyl-4-methoxybenzene (500 mg, 3.78 mmol) were dissolved in dry triethylamine (15 mL) and dry THF (15 mL). The solution was degassed with N_2 for 20 min. $Pd(PPh_3)_2Cl_2$ (80.0 mg, 0.114 mmol) and CuI (22.0 mg, 0.116 mmol) were then added to the mixture and the solution was stirred overnight at 70 °C under N_2. The reaction mixture was cooled to room temperature, diluted with water (30 mL) and washed with DCM (3 × 30 mL). The organic extracts were combined, dried over $MgSO_4$, filtered, and the solvent evaporated under reduced pressure. The crude product was purified by column chromatography (SiO_2, petroleum ether:DCM; 1:1) to give **3** as a yellow solid (735 mg, 56%); M.p. 122–123 °C; ^{1}H NMR (500 MHz, $CDCl_3$) δ = 3.85 (3H, s), 6.90–6.92 (2H, m), 7.58–7.61 (2H, m), 7.63 (1H, d, *J* = 7.6 Hz), 7.82 (1H, d, *J* = 7.6 Hz); ^{13}C NMR (125 MHz, CDCl3) δ = 55.4, 83.5, 97.2, 114.1, 114.1, 114.5, 117.1, 132.0, 132.4, 133.6, 153.1, 154.2, 160.3; HRMS (*m/z*) (EI^+): calcd. for $C_{15}H_9N_2OS^{79}Br$: 343.9619; found: 343.9618 [M^+]; *ν* max (solid state): 1606, 1576, 1531, 1504, 1483, 1288, 1246, 1169, 1027, 936, 882, 840, 840, 821 cm^{-1}.

3.2.2. Compound **6**

Compound **2**[21] (1.67 g, 5.67 mmol) and compound **5** (560 mg, 3.78 mmol) were dissolved in dry triethylamine (15 mL) and dry THF (15 mL). The solution was degassed with N_2 for 20 min. $Pd(PPh_3)_2Cl_2$ (80.0 mg, 0.114 mmol) and CuI (22.0 mg, 0.116 mmol) were then added to the mixture and the solution was stirred overnight at 70 °C under N_2. The reaction mixture was then cooled to room temperature, diluted with water (30 mL), and washed with DCM (3 × 30 mL). The organic extracts were combined, dried over $MgSO_4$, filtered, and the solvent evaporated under reduced pressure. The crude product was purified by column chromatography (SiO_2, petroleum ether:DCM; 2:1) to give **6** as a yellow solid (618 mg, 45%); M.p. 146–147 °C; ^{1}H NMR (500 MHz, $CDCl_3$) δ = 2.51 (3H, s), 7.23 (2H, d, *J* = 8.5 Hz), 7.56 (2H, d, *J* = 8.5 Hz), 7.64 (1H, d, *J* = 7.6 Hz), 7.83 (1H, d, *J* = 7.6 Hz); ^{13}C NMR (125 MHz, $CDCl_3$) δ = 31.6, 84.7, 96.9, 114.5, 116.8, 118.5, 125.7, 132.0, 132.2, 132.6, 140.7, 153.1, 154.2; HRMS (*m/z*) (EI^+): calcd. for $C_{15}H_9N_2S_2^{79}Br$: 359.9391; found: 359.9386 [$M]^+$; ν_{max} (solid state): 2970-2920, 1490, 1365, 1217, 1095, 937, 880, 841, 813, 803 cm^{-1}.

3.2.3. Compound **9**[22]

Compound **2**[21] (1.52 g, 5.17 mmol), and compound **8** (500 mg, 3.44 mmol) were dissolved in dry triethylamine (20 mL) and dry THF (10 mL). The solution was degassed with N_2 for 20 min. $Pd(PPh_3)_2Cl_2$ (73.0 mg, 0.104 mmol), and CuI (20.0 mg, 0.105 mmol) were then added to the mixture and the solution was stirred at 70 °C for 6 h under N_2. The reaction mixture was then cooled to room temperature, diluted with water (30 mL), and washed with DCM (3 × 30 mL). The organic extracts were combined, dried over $MgSO_4$, filtered, and the solvent evaporated under reduced pressure. The crude product was purified by column chromatography (SiO_2, petroleum ether: DCM; 2:1) to give **9** as a red solid (663 mg, 54%); M.p. 150–152 °C; ^{1}H NMR (500 MHz, $CDCl_3$) δ = 3.02 (6H, s), 6.66–6.69 (2H, m), 7.51–7.54 (2H, m), 7.59 (1H, d, *J* = 7.6 Hz), 7.80 (1H, d, *J* = 7.6 Hz); ^{13}C NMR (125 MHz, $CDCl_3$) δ = 40.1, 83.2, 99.1, 108.9, 111.7, 113.1, 117.8, 131.7, 132.1, 133.3, 150.6, 153.1, 154.3; HRMS (*m/z*) (EI^+): $[M]^+$; calcd. for $C_{16}H_{12}N_3S^{79}Br$ requires 356.9935; found 356.9937.

3.2.4. Compound **4**

Compound **3** (600 mg, 1.74 mmol), 4-formylphenylboronic acid (310 mg, 2.09 mmol) and potassium carbonate (2.40 g, 17.4 mmol) were dissolved in THF (25 mL) and water (9 mL). The solution was degassed with N_2 for 20 min. Tetrakis(triphenylphosphine)palladium(0) (100 mg, 0.142 mmol) was then added to the mixture and the solution was stirred overnight at 70 °C under N_2. The reaction mixture was then cooled to room temperature, diluted with water (20 mL) and washed with DCM (3 × 30 mL). The organic extracts were combined, dried over $MgSO_4$, filtered, and the solvent evaporated under reduced pressure. The crude product was purified by column chromatography (SiO_2, petroleum ether:DCM; 1:1) to give **4** as a yellow solid (625 mg, 97%); M.p. 181–182 °C; ^{1}H NMR (500 MHz, $CDCl_3$) δ = 3.85 (3H, s), 6.91–6.94 (2H, m), 7.60–7.64 (2H, m), 7.76 (1H, d, *J* = 7.5 Hz), 7.86 (1H, d, *J* = 7.5 Hz), 8.02–8.05 (2H, m), 8.13–8.16 (2H, m), 10.10 (1H, s); ^{13}C NMR (125 MHz, $CDCl_3$) δ = 55.4, 84.2, 97.3, 114.1, 114.6, 117.7, 128.5, 129.8, 130.0, 132.2, 133.6, 132.4, 136.0, 142.9, 152.9, 155.3, 160.3, 181.8; HRMS (*m/z*) (EI^+): calcd. for $C_{22}H_{14}N_2O_2S$: 370.0776; found: 370.0765 $[M]^+$; ν_{max} (solid state): 2924-2753, 1691, 1599, 1540, 1507, 1244, 1213, 1159, 1033, 1023, 890, 837, 827 cm^{-1}.

3.2.5. Compound **7**

Compound **6** (300 mg, 0.830 mmol), 4-formylphenylboronic acid (150 mg, 1.00 mmol) and potassium carbonate (1.2 g, 8.3 mmol) were dissolved in THF (15 mL) and water (5 mL). The solution was degased with N_2 for 20 min. Tetrakis(-triphenylphosphine)palladium(0) (100 mg, 0.142 mmol) was then added to the mixture and the solution was stirred overnight at 70 °C under N_2. The reaction mixture was then cooled to room temperature, diluted with water (20 mL), and washed with DCM (3 × 30 mL). The organic extracts were combined, dried over $MgSO_4$, filtered, and the solvent evaporated under reduced pressure. The crude product was purified by column chromatography (SiO_2, petroleum ether:DCM; 1:1) to give **7** as a yellow solid (272 mg, 85%); M.p. 166–167 °C; ^{1}H NMR (500 MHz, $CDCl_3$) δ = 2.52 (3H, s), 7.25 (2H, d, *J* = 8.4 Hz), 7.59 (2H, d, *J* = 8.4 Hz), 7.78 (1H, d, *J* = 7.4 Hz), 7.89 (1H, d, *J* = 7.4 Hz), 8.05 (2H, d, *J* = 8.2 Hz), 8.15 (2H, d, *J* = 8.2 Hz), 10.11 (1H, s); ^{13}C NMR (125 MHz, $CDCl_3$) δ = 14.2, 85.4, 96.9, 117.4, 118.6, 125.7, 128.4, 129.8, 130.0, 132.3, 132.6, 132.8, 136.0, 140.6, 142.8, 152.9, 155.2, 191.9; HRMS (*m/z*) (EI^+): calcd. for $C_{22}H_{14}N_2OS_2$: 386.0548; found: 386.0556 $[M]^+$; ν_{max} (solid state): 2916-2822, 1692, 1600, 1540, 1490, 1212, 1090, 888, 823, 817 cm^{-1}.

3.2.6. Compound ***10***

Compound **9** (300 mg, 0.84 mmol), 4-formylphenylboronic acid (150 mg, 1.00 mmol) and potassium carbonate (120 mg, 8.40 mmol) were dissolved in THF (15 mL) and water (5 mL). The solution was degassed with N_2 for 20 min. Tetrakis(triphenylphosphine)palladium(0) (100 mg, 0.142 mmol) was then added to the mixture and the solution was stirred overnight at 70 °C under N_2. The reaction mixture was cooled to room temperature, diluted with water (20 mL), and washed with DCM (3 × 30 mL). The organic extracts were combined, dried over $MgSO_4$, filtered, and the solvent evaporated under reduced pressure. The crude product was purified by column chromatography (SiO_2, petroleum ether: DCM; 1:1) to give **10** as a yellow solid (239 mg, 74%); M.p. 209–210 °C; ^{1}H NMR (500 MHz, $CDCl_3$) δ = 3.02 (6H, s), 6.77–6.79 (2H, m), 7.54–7.57 (2H, m), 7.75 (1H, d, *J* = 7.4 Hz), 7.82 (1H, d, *J* = 7.4 Hz), 8.03 (2H, d, *J* = 8.3 Hz), 8.14 (2H, d, *J* = 8.3 Hz), 10.10 (1H, s); ^{13}C NMR (125 MHz, $CDCl_3$) δ = 40.1, 84.0, 99.2, 111.7, 109.0, 118.4, 128.6, 129.8, 129.9, 131.7, 133.3, 131.3, 131.6, 143.0, 150.6, 152.9, 155.3, 191.8; HRMS (*m/z*) (EI^+): calcd. for $C_{23}H_{17}N_3OS$ 383.1092; found: 383.1080 $[M]^+$; ν_{max} (solid state): 2892-2716, 1694, 1602, 1539, 1517, 1351, 1217, 1155, 830, 815 cm^{-1}.

3.2.7. Compound ***LS-385***

Compound **4** (300 mg, 0.810 mmol), cyanoacetic acid (83 mg, 0.97 mmol), piperidine (8.0 μl, 0.081 mmol), acetic acid (37 μl, 0.65 mmol) and $MgSO_4$ (40 mg, 0.16 mmol) were stirred in dry-toluene (40 mL) and the solution was heated at 80 °C for 2 h under N_2. The reaction was then cooled to room temperature. The resulting precipitate was filtered and washed with petroleum ether (3 × 20 mL) and with water (3 × 20 mL). Recrystallization from methanol gave **LS-385** as an orange solid (255 mg, 72%); M.p. 209–210 °C; δ = 3.83 (3H, s), 7.03–7.06 (2H, m), 7.58–7.62 (2H, m), 8.00 (1H, d, *J* = 7.5 Hz), 8.03 (1H, d, *J* = 7.5 Hz), 8.17–8.20 (2H, m), 8.23–8.25 (2H, m), 8.38 (1H, s); ^{13}C NMR (125 MHz, DMSO-d_6) δ = 55.8, 85.1, 96.9, 105.5, 114.2, 115.1, 116.6, 116.9, 129.1, 130.2, 131.2, 132.2, 133.8, 153.3, 132.1, 133.1, 152.7, 140.8, 155.0, 160.6, 163.7; HRMS (*m/z*) ($nESI^-$): calcd. for $C_{25}H_{14}N_3O_3S$: 436.0761; found 436.0756 $[M-H]^-$; ν_{max} (solid state): 3252-2716 (br), 2363, 1702, 1604, 1591, 1543, 1508, 1422, 1289, 1250, 1195, 1161, 1034, 1022, 891, 827 cm^{-1}.

3.2.8. Compound ***LS-386***

Compound **7** (200 mg, 0.520 mmol), cyanoacetic acid (53 mg, 0.62 mmol), piperidine (8 μl, 0.052 mmol), acetic acid (24 μl, 0.41 mmol) and $MgSO_4$ (26 mg, 0.10 mmol) were stirred in dry-toluene (30 mL) and the solution was heated at 80 °C for 2 h under N_2. The reaction mixture was then cooled to room temperature. The resulting precipitate was filtered and washed with petroleum ether (3 × 20 mL) and with water (3 × 20 mL). Recrystallization from methanol gave **LS-386** as an orange solid (162 mg, 69%); M.p. 219–220 °C; ^{1}H NMR (500 MHz, DMSO-d_6) δ = 2.54 (3H, s), 7.35 (2H, d, *J* = 8.3 Hz), 7.58 (2H, d, *J* = 8.3 Hz), 8.01–8.06 (2H, m), 8.17 (2H, d, *J* = 8.2 Hz), 8.23 (2H, d, *J* = 8.2 Hz), 8.31 (1H, s); ^{13}C NMR (125 MHz, DMSO-d_6) δ = 44.1, 86.3, 96.5, 116.2, 117.5, 126.1, 129.0, 133.4, 130.2, 130.9, 132.4, 118.1, 132.6, 151.9, 140.4, 141.2, 147.1, 152.0, 152.8, 155.0, 163.5; HRMS (*m/z*) ($nESI^-$): calcd. for $C_{25}H_{14}N_3O_2S_2$: 452.0533; found 452.0536 $[M-H]^-$; ν_{max} (solid state): 3209-2712 (br), 2362, 1708, 1594, 1542, 1492, 1423, 1273, 1222, 1198, 1093, 894, 852, 824 cm^{-1}.

3.2.9. Compound ***LS-387***

Compound **10** (200 mg, 0.520 mmol), cyanoacetic acid (53 mg, 0.62 mmol), piperidine (8 μl, 0.052 mmol), acetic acid (24 μl, 0.41 mmol) and $MgSO_4$ (26 mg, 0.10 mmol) were stirred in dry-toluene (30 mL) and the solution was heated at 80 °C for 2 h under N_2. The reaction mixture was cooled to room temperature. The resulting precipitate was filtered and washed with petroleum ether (3 × 20 mL) and with water (3 × 20 mL). Recrystallization from methanol gave **LS-387** as a red solid (162 mg, 69%); M.p. 232–233 °C (dec.); ^{1}H NMR (500 MHz, DMSO-d_6) δ = 3.00 (6H, s), 6.77 (2H, d, *J* = 8.7 Hz), 7.47 (2H, d, *J* = 8.7 Hz), 7.94 (1H, d, *J* = 7.3 Hz), 8.02 (1H, d, *J* = 7.3 Hz), 8.20 (2H, d, *J* = 8.3 Hz), 8.26 (2H, d, *J* = 8.3 Hz), 8.38 (1H, s); ^{13}C NMR (125 MHz, DMSO-d_6) δ = 40.1, 84.8, 99.0, 112.4, 108.2, 117.4, 129.2, 130.1, 131.2, 131.4, 132.0, 132.2, 133.3, 153.3, 140.9, 151.0, 152.8, 153.3, 155.0, 158.2, 164.0; HRMS (*m/z*) ($nESI^-$): calcd. for $C_{26}H_{17}N_4O_2S$: 449.1078; found: 449.1080 $[M-H]^-$; ν_{max} (solid state): 3131-2716 (br), 2353, 1726, 1694, 1605, 1538,1433, 1422, 1365, 1354, 1281, 1227, 1199, 1156, 942, 894, 834, 820 cm^{-1}.

3.3. Computation

Density functional theory (DFT) and time-dependent density functional theory (TDDFT) calculations were performed with Gaussian '09 package.[23] All geometries were optimized using Becke's three-parameter hybrid and Lee-Yang-Parr's gradient corrected correlation (B3LYP) functional and 6-311G (d, p) basis set without additional diffused function. None of the vibrational frequencies in the optimized geometries generated negative frequencies in their ground state. The excitation energies and oscillator strengths were determined by using TDDFT under CAM-B3LYP functional and 6–311++G (d, p) basis set level of theory on the basis of the optimized ground state geometries. A solvation model (acetonitrile: ε = 35.688) was applied for TDDFT calculations by means of polarizable continuum model (PCM) method.

3.4. DSSC fabrication and measurements

The inverse micelles containing ytterbium (III) chloride were spin-coated onto transparent fluorine-doped SnO_2 (FTO)-coated conducting glass (TEC 8, Pilkington, Sheet resistance = 8 Ω/sq) at 2000 rpm for 60 s. The zero-dimensional ytterbium oxide nanodots on the substrate were formed after eliminating the polymer template by O_2 plasma etching. More details about their preparation can be found in the literature.[24] 20 nm-TiO_2 Photoanodes were screen-printed on the ytterbium oxide nanodot arrays and the resulting layers were sintered at 575 °C for 3 h in a muffle furnace. Subsequently, 400 nm-TiO_2 scattering layers were screen-printed

on the photoanodes and then thermally sintered at 575 °C for 3 h in a muffle furnace. Active areas of the electrodes were 0.20 cm^2. The prepared TiO_2 electrodes were immersed in a 0.04 M $TiCl_4$ solution at 75 °C for 30 min. They were rinsed with deionized water and ethanol and then sintered at 500 °C for 30 min on a hot plate. The electrodes were exposed to O_2 plasma for 10 min and then immersed into a 0.5 mM photosensitizer (**N719**, **LS-385**, **LS-386**, and **LS-387**) solution in ethanol. Pt counter electrodes were prepared by thermal reduction of 20 mM chloroplatinic acid (H_2PtCl_6, Sigma-Aldrich) in 2-propanol at 550 °C for 1 h. Both the photosensitizer-anchored photoanode and the platinum counter electrode were assembled using a 25 μm-thick thermoplastic Surlyn (Solaronix). A commercially available iodide electrolyte (AN-50, Solaronix) was filled through the pre-drilled holes in the counter electrode.

The photovoltaic characteristics of the devices were measured by using a solar cell I-V measurement system (K3000 LAB, McScience, Korea) under both AM1.5 global one sun illumination (100 mW/cm^2) and dark conditions. Short-circuit photocurrent density (J_{sc}), open-circuit voltage (V_{oc}), fill factor (FF) and power conversion efficiency (η) were measured simultaneously. Monochromatic incident photon-to-current conversion efficiency (IPCE) was recorded to evaluate the spectral response of solar cells (K3100, McScience, Korea). Electrochemical impedance spectroscopy (EIS) measurements were performed with DSSCs biased to V_{oc} under illumination and in dark by using a frequency response analyzer (Solartron 1260). A sinusoidal potential perturbation with an amplitude of 100 mV was applied over a frequency range of 0.1 Hz–100 kHz.

4. Conclusion

We report the synthesis of 'D-π-A_1-π-A_2' metal-free organic dyes featuring MeO-, MeS- and Me_2N- as donor residues. The strong donor ability of the Me_2N- unit made **LS-387** possess high light harvesting and electron injection abilities and thus DSSCs sensitized with this dye exhibited the best photovoltaic performance ($\eta = 5.61\%$) among the three photosensitizers. Although the DSSC performance of **LS-387** was lower than that of **N719** ($\eta = 8.16\%$), further optimization (e.g. film thickness, electrolyte, addition of co-additives) should result in better DSSC performance.

Acknowledgements

GC thanks the EPSRC for funding (EP/E036244/1). JH acknowledges the Chung-Ang University Research Grants in 2016 and the Energy Technology Development program through the Korea Institute of Energy Technology Evaluation and Planning (KETEP) funded by the Ministry of Trade, Industry and Energy (MOTIE) of Korea (No. 201502000920).

Appendix A. Supplementary data

Supplementary data related to this article can be found at http://dx.doi.org/10.1016/j.tet.2016.12.061.

References

1. O'Regan B, Grätzel M. *Nature*. 1991;353:737–740.
2. Hagfeldt A, Boschloo G, Sun L, Kloo L, Pettersson H. *Chem Rev*. 2010;110:6595–6663.
3. (a) Mishra A, Fischer MK, Bäuerle P. *Angew Chem Int Ed*. 2009;48:2474–2499;
(b) Ooyama Y, Harima Y. *ChemPhysChem*. 2012;13:4032–4080;
(c) Kanaparthi RK, Kandhadi J, Giribabu L. *Tetrahedron*. 2012;68:8383–8393;
(d) Kim BG, Chung K, Kim J. *Chem Eur J*. 2013;19:5220–5230.
4. Kloo L. *Chem Comm*. 2013;49:6580–6583.
5. Liang M, Chen J. *Chem Soc Rev*. 2013;42:3453–3488.
6. Tseng CY, Taufany F, Nachimuthu S, Jiang JC, Liaw DJ. *Org Electron*. 2014;15:1205–1214.
7. Wu Y, Zhu W. *Chem Soc Rev*. 2013;42:2039–2058.
8. (a) Ying W, Guo F, Li J, et al. *ACS Appl Mater Interfaces*. 2012;4:4215–4224;
(b) Zhu W, Wu Y, Wang S, et al. *Adv Funct Mater*. 2011;21:756–763;
(c) Lan T, Lu X, Zhang L, Chen Y, Zhou G, Wang ZS. *J Mater Chem A*. 2015;3:9869–9881;
(d) Li X, Zheng Z, Jiang W, Wu W, Wang Z, Tian H. *Chem Comm*. 2015;51:3590–3592;
(e) Khanasa T, Prachumrak N, Kochapradist P, et al. *Tetrahedron Lett*. 2014;55:3244–3248.
9. (a) Xu W, Peng B, Chen J, Liang M, Cai F. *J Phys Chem C*. 2008;112:874–880;
(b) Baheti A, Singh P, Lee CP, Thomas KJ, Ho KC. *J Org Chem*. 2011;76:4910–4920;
(c) Tarsang R, Promarak V, Sudyoadsuk T, Namuangruk S, Jungsuttiwong S. *J Photochem Photobiol A Chem*. 2014;273:8–16;
(d) Mahmood A. *Sol Energy*. 2016;123:127–144.
10. (a) Teng C, Yang X, Yang C, et al. *J Phys Chem C*. 2010;114:11305–11313;
(b) Song JL, Amaladass P, Wen SH, et al. *New J Chem*. 2011;35:127–136.
11. Bredas JL. *Mater Horizons*. 2015;1:17–19.
12. Glockler G. *J Phys Chem*. 1958;62:1049–1054.
13. Kręglewski M. *J Mol Spectrosc*. 1989;133:10–21.
14. Stevenson D, Beach J. *J Am Chem Soc*. 1938;60:2872–2876.
15. Mo Y, Lin Z, Wu W, Zhang Q. *J Phys Chem*. 1996;100:11569–11572.
16. Seo D, Park K-W, Kim J, Hong J, Kwak K. *Comp Theor Chem*. 2016;1081:30–37.
17. Böhm S, Exner O. *J Mol Struct THEOCHEM*. 2005;722:125–131.
18. Rolczynski BS, Szarko JM, Son HJ, Liang Y, Yu L, Chen LX. *J Am Chem Soc*. 2012;134:4142–4152.
19. Rühle S, Greenshtein M, Chen SG, et al. *J Phys Chem B*. 2005;109:18907–18913.
20. Wang Q, Moser JE, Grätzel M. *J Phys Chem B*. 2005;109:14945–14953.
21. Sun YQ, He J, Xu Z, et al. *Chem Comm*. 2007:4779–4781.
22. Chen S, Li Y, Yang W, Chen N, Liu H, Li Y. *J Phys Chem C*. 2010;114:15109–15115.
23. Frisch MJ, Trucks GW, Schlegel HB, et al. *Gaussian 09*. Wallingford CT: Gaussian, Inc; 2009.
24. Park K-W, Ahn S, Lim SH, et al. *Appl Surf Sci*. 2016;364:573–578.